Макрогетероциклы
http://macroheterocycles.isuct.ru

DOI: 10.6060/mhc200501s

Коньюгаты цинкового комплекса тетраметилпиридилпорфирина с коллоидными наночастицами золота стабилизированными цитратом

О. М. Куликова,[a] В. Б. Шейнин,[a@] О. И. Койфман[a,b]

[a]*Институт химии растворов им. Г. А. Крестова РАН, 153045 Иваново, Россия*
[b]*Ивановский государственный химико-технологический университет, 153000 Иваново, Россия.*
[@]*E-mail: vbs@isc-ras.ru*

При электростатическом взаимодействии коллоидных наночастиц Au_{30900}/Cit с цинковым комплексом 5,10,15,20-тетракис(4'-N-метилпиридил)порфина друг за другом образуются два различных наноконъюгата постоянного состава со спектрами поглощения, отличными от спектров исходных реагентов. Образование первого, более прочного, соединения сопровождается падением интенсивности и красным сдвигом полос Соре и полосы поверхностного плазмонного резонанса (ППР) конъюгированных реагентов, которые сохраняют свою спектральную идентичность. Образование второго коньюгата сопровождается ростом интенсивности полосы Соре, в то время как полоса ППР практически не меняется. Высказано предположение о том, что первым образуется наноконъюгат только с одним тетракатионом, который понижает способность наночастицы к дальнейшей конъюгации.

Ключевые слова: Наночастицы золота, тетра(N-метилпиридил)порфин, цинковый комплекс, гибридные органо-неорганические конъюгаты.

Conjugates of Zinc Tetramethylpyridylporphyrinate with Colloidal Gold Nanoparticles Stabilized with Citrate

Olga M. Kulikova,[a] Vladimir B. Sheinin,[a@] and Oscar I. Koifman[a,b]

[a]*G.A. Krestov Institute of Solution Chemistry of the Russian Academy of Sciences, 153045 Ivanovo, Russia*
[b]*Ivanovo State University of Chemistry and Technology, 153000 Ivanovo, Russia*
[@]*Corresponding author E-mail: vbs@isc-ras.ru*

Due to electrostatic interaction of Au_{30900}/Cit colloidal nanoparticles with 5,10,15,20-tetrakis(4'-N-methylpyridyl) porphine complex with zinc two different nanoconjugates of constant composition are formed one after another, the UV-Vis spectra of which differ from those of initial reagents. The formation of the first, more stable, compound is accompanied by a decrease in intensity and a red shift of the Soret band and SPR band of the conjugated reagents, which retain their spectral identity. The formation of the second conjugate is accompanied by an increase in the intensity of the Soret band while the SPR band is not changed significantly. It has been suggested the nanoconjugate with only one tetracation to form first, which reduces the nanoparticle ability to further conjugation.

Keywords: Gold nanoparticles, tetra(N-methylpyridyl)porphine, zinc complex, organic-inorganic hybrid nanoconjugates.

Introduction

Developing a theranostic platform that integrates the targeted drug delivery, diagnostic and therapeutic functions is a great challenge of modern personalized nanomedicine. At the drug delivery stage it is important, on the one hand, to temporarily suppress the drug activity, since it can lead to healthy tissues and blood cells damage, and on the other hand, to ensure the drug targeting with recovery of all necessary functions in the lesion.[1–5]. When developing such a system, the optimal solution would be to use a substance that would simultaneously provide suppression of therapeutic agent activity and its targeted delivery to the damaged tissue. The specific and essential functions that porphyrins and related compounds perform in nature have attracted the constant attention of researchers, with the aim to create effective molecular systems, demanded in various fields of diagnostic and therapeutic medicine, as well as the creation of new nanomaterials using bottom-up technology.

Porphyrins and their derivatives are well-known photosensitizers (PS) of first and second generations used in photodynamic therapy (PDT) and antimicrobial therapy.[6–14] Moreover, porphyrin compounds possess the antimicrobial and antivirus activity and have been tested against HIV and coronavirus.[15–20] Currently, the construction and study of nano-sized organo-inorganic conjugates are the main tasks in the development of functional systems for chemosensorics, catalysis, molecular electronics, nanobiomedicine.[21–28] Gold and silver nanoparticles are a type of inorganic nanoparticles that are currently being widely studied for biomedicine applications.[29–31] Such properties as tunable size and shape, possibility of surface modification, biocompatibility, and ability to interact with active ligands make it possible to consider noble metals nanoparticles as promising drug carriers in anticancer and antibacterial theranostics.[32–37] The reason for the increased attention to such objects is the unique photophysical property called localized surface plasmon resonance (LSPR). Nowadays LSPR phenomenon is widely used for chemical and biological sensing applications. Contacting with biological objects, plasmon effects make it possible to increase the fluorescence intensity by more than an order of magnitude, greatly expands the possibilities of detection, identification, diagnosis and therapy. [38] Surface plasmon resonance induction leads not only to a significant increase in light absorption/scattering, but can also result in nanoparticles heating. In PDT using such NPs as a part of composite PS can lead to combine PDT and PTT (photothermal therapy) effect and to broad the PDT scope in cancer treatment.[39] The ability to use nanoparticles as a link for PDT and PTT was discussed in [40,41] The area of developing therapeutic agents for PDT based on noble metals nanoparticles and macrocyclic PS, such as Zn-phthalocyanine derivatives,[42–45] Si-phthalocyanine,[46–48] hematoporphyrin,[49] meso-tetra(4-carboxyphenyl)porphyrin,[50] chlorin e6,[51,52] is growing rapidly, some of obtained preparations are at the stage of clinical trials. Therefore, for the further successful development of such promising area as using conjugates of nanoparticles with macrocyclic PS, careful study of the effects caused by interaction of these objects in aqueous solutions is necessary. Modern trends indicate that the further research direction will focus on the creation the next generation of theranostic agents based on porphyrins and metal nanoparticles (AuNP). The concept of a theranostic platform developing based on multifunctional porphyrin nanostructures will enhance the abilities of modern medicine and allow for a shift to modern personalized nanomedicine. [53]

This work is devoted to water-soluble hybrid nanoconjugates, which are formed during the interaction of readily available reagents: colloidal gold nanoparticles and zinc complex of tetramethylpyridylporphyrin

Experimental

Chemicals and materials

All commercially available solvents and reagents were used without further purification: 4-Pyridinecarboxaldehyde (98 %, Acros Organics); 2,3-Dichloro-5,6-dicyano-*p*-benzoquinone (98 %, Sigma-Aldrich), pyrrole (reagent grade, 98 %, Sigma-Aldrich), methyl iodide (≥ 99.0 %, Sigma-Aldrich); perchloric acid (70 %, ASC reagent, Aldrich), hydrogen tetrachloroaurate (III) ($HAuCl_4 \cdot 3H_2O$, > 99.99 %, Sigma-Aldrich), sodium citrate ($Na_3C_6H_5O_7 \cdot 2H_2O$, ≥ 99 %, Sigma-Aldrich), zinc iodide (reagent grade, LLC "Himmed"), distilled water (ISC RAS), N,N-Dimethylformamide (max. 0.01 % water, Panreac).

Water-soluble *meso*-tetra(N-methyl-4-pyridyl)porphine tetraiodide salt $\mathbf{H_2P}(PyMe^+)_4(J^-)_4$ was obtained from 5,10,15,20-tetra(4-pyridyl)porphine by quaternization of the pyridyl N-atoms with methyl iodide in DMF.[54] Initial $\mathbf{H_2P}(Py)_4$ was obtained by condensation of pyrrole with benzaldehyde in propionic acid.[55]

Zinc complex of porphyrin $\mathbf{ZnP}(PyMe^+)_4(J^-)_4$, was prepared from $\mathbf{H_2P}(PyMe^+)_4(J^-)_4$ and zinc iodide in DMF.[56,57]

A colloidal aqueous solution of gold nanoparticles stabilized by citrate anions (Au/Cit) with a SPR band maximum at 520 nm was obtained from tetrachloroauric(III) acid and sodium citrate by Frens method.[58,59]

Methods

Interaction between Au/Cit colloidal nanoparticles and $\mathbf{ZnP}(PyMe^+)_4$ tetracations was investigated by spectropotentiometric titration at 25 °C in 1 cm ×1 cm optical quartz cells using a two-channel spectrometer (Avantes AvaSpec 2048-2, Netherlands) equipped with a qpod© (Temperature-Controlled Sample Compartment for Fiber Optic Spectroscopy), pH-150MI pH meter (Izmeritelnaya Technika, Russia) with InLab Micro pH electrode (Mettler-Toledo Inc.) and micropipette with scale division value $6.3 \cdot 10^{-6}$ ml.[5,60]

Results and discussion

Characterization of colloidal nanoparticles Au/Cit

In this work pH-neutral aqueous solutions of colloidal Au/Cit nanoparticles with optical density up to 0.48 at SPR band maximum (520 nm) were used (Figure 1a). In this absorbance range the solution obey the linear Beer law $A = \varepsilon lC$ (Supporting Materials, Figure SI 1b), which indicate the absence of Au/Cit association and validity of optical density for determining the molar concentration of nanoparticles solutions.

The extinction coefficient ε_{520} of a Au/Cit nanoparticles colloidal solution, as well as the particle diameter, were

determined from the ratio of the absorbance at the SPR peak to the absorbance at 450 nm.[61,62] The experimental value A_{520}/A_{450} = 1.56 (blue line, Figure 1c) corresponds to pseudospherical Au/Cit nanoparticles with a core diameter of 12 nm (Figure 2) and the extinction coefficient of the colloidal solution $\varepsilon_{520} = 1.70 \cdot 10^8$. In this case, the thermodynamically stable crystalline form of a gold core having a diameter of 12nm is a cuboctahedron[59,63] with a face-centered cubic lattice. The closest to this value is the Au_{30900} cuboctahedron with a diameter of 12.12 nm (Figure 2), which surface consists of eight triangular Au{111} and six square Au{100} faces with a side of 6.06 nm.

Colloidal Au/Cit nanoparticles consist of a metal core and a solubilizing citrate ligands shell. Carboxylate groups provide the anchoring bond of ligands with Au^0 atoms on the core surface, as well as the solubility and aggregation stability of Au/Cit nanoparticles in water. There is no quantitative information on the stoichiometry, structure, and ligands shell charge of colloidal Au/Cit nanoparticles *in situ*. It is known that the basicity of the carboxylate groups of citric acid increases in the series (1):[64,65]

This fact suggests that the strength of ligands bonding with the surface of the gold nanoparticle changes in the same order, and the central carboxylate is the key anchor group.[66–69]

As an illustration, Figure 3a, b shows a fragment of the Au{100} surface with a population density of 0.67 Cit/nm^2, where each ligand is linked through a central carboxylate anchor group, while two side groups remain free and act as anionic solvation centers.

In this case total amount of ligands on the surface of spherical nanoparticle Au/Cit is 303 units, which corresponds to negative charge is –909. Surface charge is in great dependence of ligands population degree. (Figure 3c). However, in any case the charge of citrate shell will be significantly lower if some of the ligands are bound to the nucleus surface by two and three carboxylate groups or protonated Ionization degree of citrate ligands is pH-dependent value. Calculation using citric acid protonation constants predicts that of the Au/Cit citrate shell protonation begins below pH 8 (Figure 4a) and finishes around pH 1. Titration of Au/Cit with perchloric acid (Figure 4b) has shown that protonation of the obtained nanoparticles begins at pH < 7, but still remain aggregation stability up to pH 2, despite the visible protolytic changes in the ligand shell, which can be checked by the SPR band response. The sensitivity of the Au/Cit nanoparticles SPR band to physicochemical processes involving the ligand shell [70] was used to study the interaction between anionic Au/Cit nanoparticles and **ZnP**$(PyMe^+)_4$ tetracation.

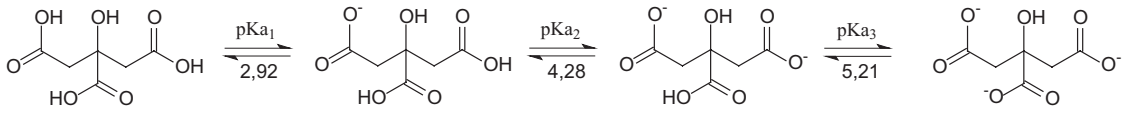

(1)

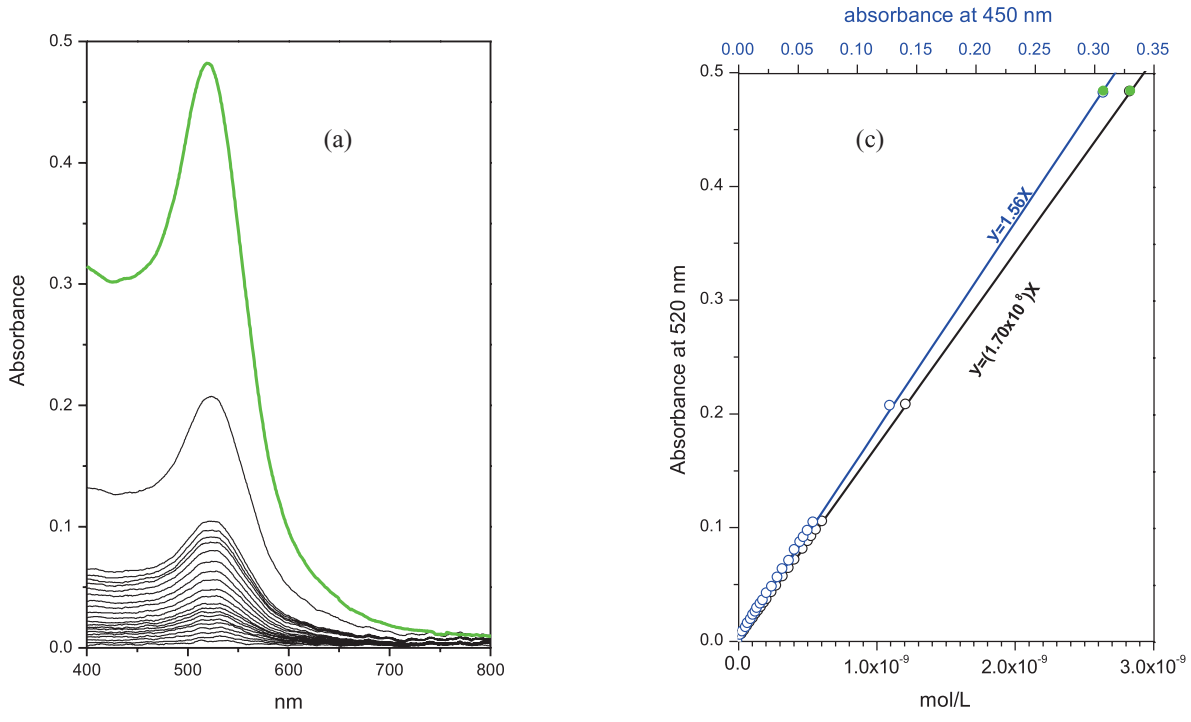

Figure 1. Absorption spectra of colloidal aqueous solutions of Au/Cit nanoparticles at different concentrations and Beer-Lambert law plots. (p*H* 7, 25 °C).

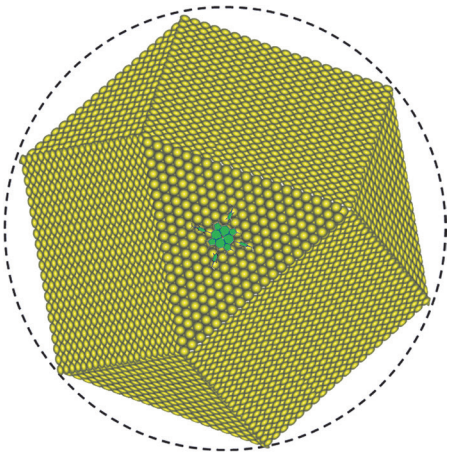

Diameter: 12.12 nm
Edge: 6.06 nm (Au_{21})
Facet Au{100}: square 36.68 nm^2(Au_{441})
Facet Au {111}: square 15.88 nm^2(Au_{231})
Surface square: 347.14 nm^2
Volume = 523.61 nm^3

Figure 2. Parameters of ideal cuboctahedral nanocrystal Au_{30900}. The size of **ZnP**$(PyMe^+)_4$ tetracation is shown in green for comparison.

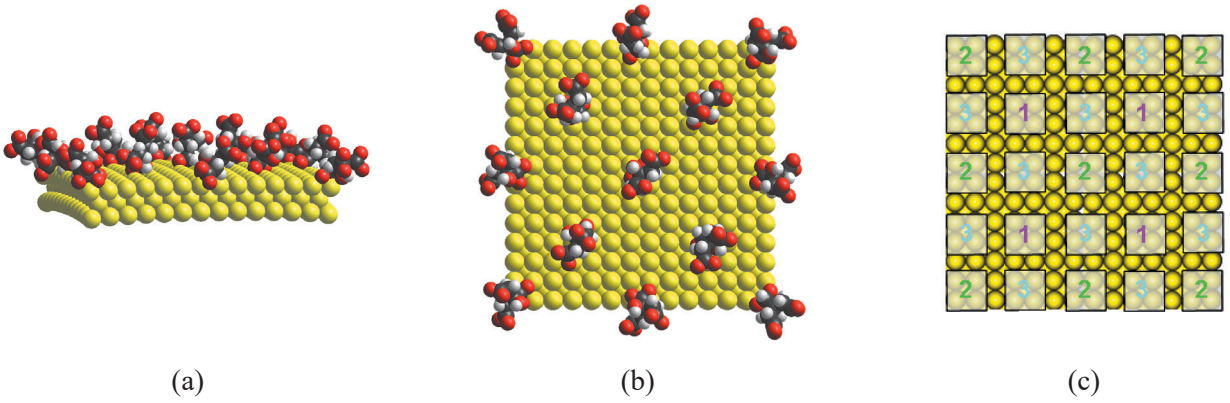

Figure 3. (a),(b) – MM + optimized fragment of Au(100) surface of spherical nanoparticle AuNP/Cit (see Figure 2b). The thickness of citrate shell is about 0.65 nm. (c) – Variants of equitable cold core surface population in Cit/nm^2: **1, 2** – 0.33, **3,** (**1** + **2**) **–** 0.67, (**1** + **3**) – 1, (**1** + **2** + **3**) – 1.34.

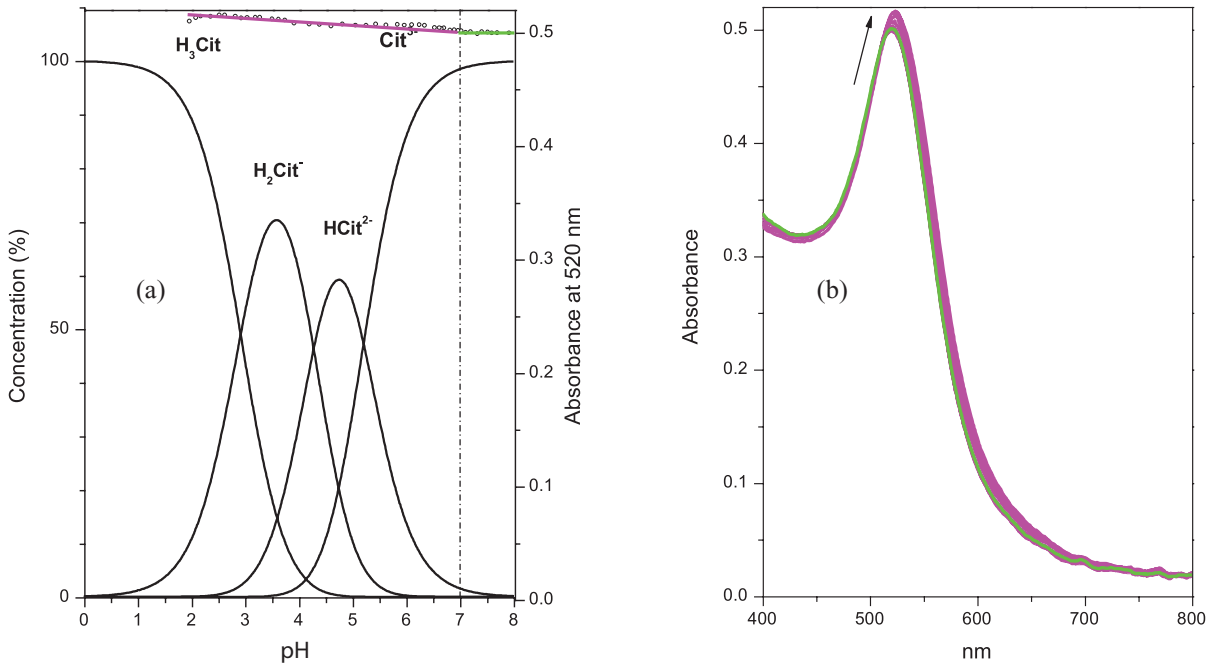

Figure 4. pH effect on the concentration of conjugated ionic forms of citric acid (a) and on the UV-Vis spectrum of a colloidal Au/Cit aqueous solution at 25 °C (b). The green line shows the absorption spectrum for the pH range 7-8, the magenta color shows the change in the absorption spectra in the pH range 2-7.

Characterization of ZnP(PyMe$^+$)$_4$ tetracation

Tetracation exists in aqueous solution as axial aqua-comples (H$_2$O)**ZnP**(PyMe$^+$)$_4$ (**Figure** 5), stable at pH range p*H*<10. At pH> 10, such aqua-complex undergo the acidic dissociation with the hydroxo-complex (OH$^-$)**ZnP**(PyMe$^+$)$_4$ formation[71].

Tetracation consists of slightly distorted porphyrin plain and four positively charged meso-substituents, which free rotation is limited by van der Waals repulsion between *ortho* and *beta*-protons. Geometrically, tetracation (H$_2$O)**ZnP**(PyMe$^+$)$_4$ can be inscribed in a square with an area of 1.72 нм^2, a side of 1.31 nm and a diagonal of 1.85 nm between methyl groups.

Aqueous solutions of **ZnP**(PyMe$^+$)$_4$ are characterized by an intense Soret band with an absorption maximum at 435 nm and a double fluorescence band with a maximum and shoulder at 635 and 663 nm, respectively (Figure 6a). Due to the high like charges, tetracations form stable molecular-dispersed solutions, which strictly obey the Beer-Lambert law in the working concentrations range up to 6·10^{-6} mol/l (Figure 6b). An important fact is that the extinction coefficient of (H$_2$O)**ZnP**(PyMe$^+$)$_4$ aqueous solution, equal to 206000 [72], is an exact tabular value in contrast to colloidal Au/Cit nanoparticles.

Interaction of AuNC/Cit with (H$_2$O)ZnP(PyMe$^+$)$_4$

During the titration of colloidal aqueous solutions of Au/Cit nanoparticles with (H$_2$O)**ZnP**(PyMe$^+$)$_4$ tetracations, two different types of conjugates were stepwise obtained, and their UV-Vis spectra are differ from the spectra of initial compounds (Figure 7a).

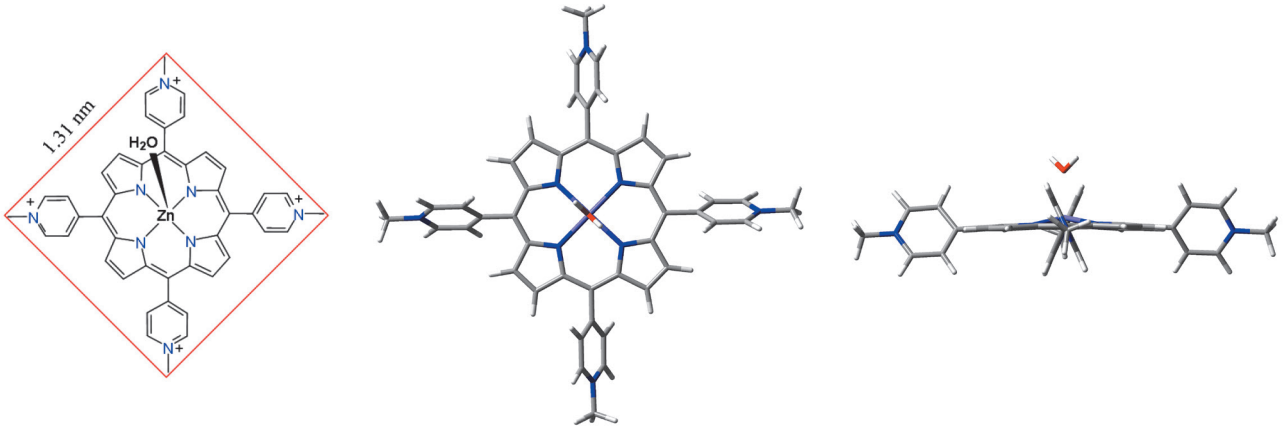

Figure 5. Molecular geometry of (H$_2$O)**ZnP**(PyMe$^+$)$_4$ tetracation optimized by DFT/B3LYP/631G/(d,p).

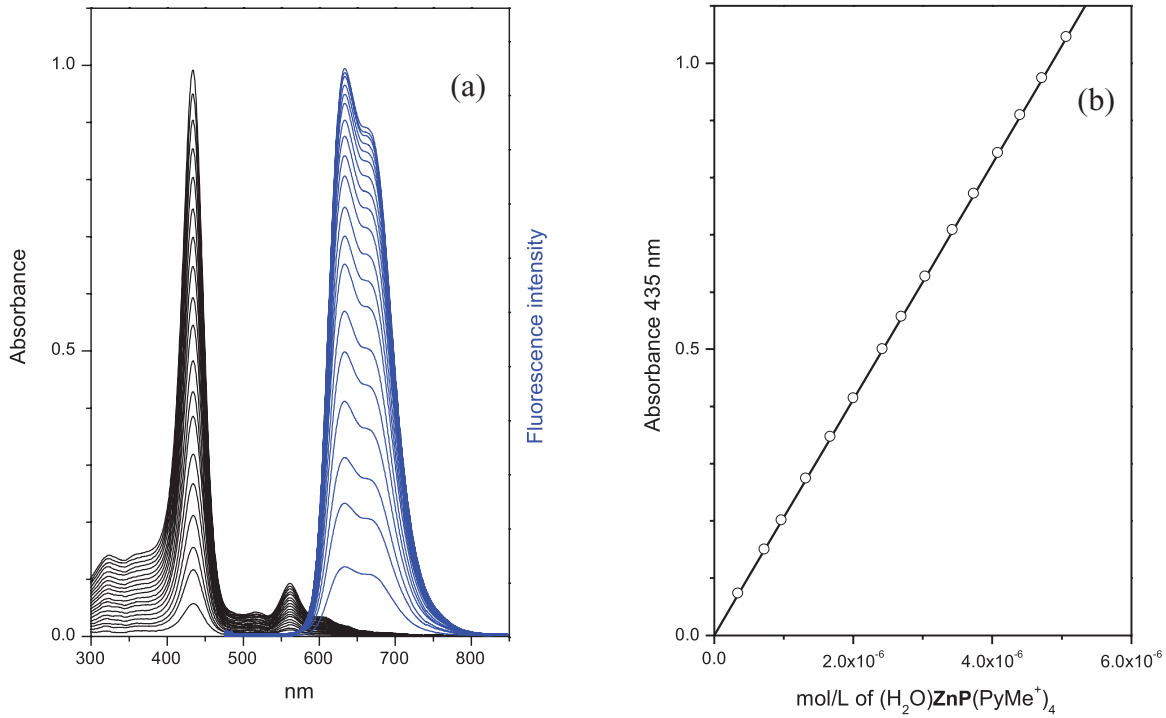

Figure 6. UV-Vis spectra of pH-neutral aqueous solution of (H$_2$O)**ZnP**(PyMe$^+$)$_4$ tetracation at different concentrations, 25 °C (a) and the Beer-Lambert law plot (b), extinction ε_{435} = 206000.[72]

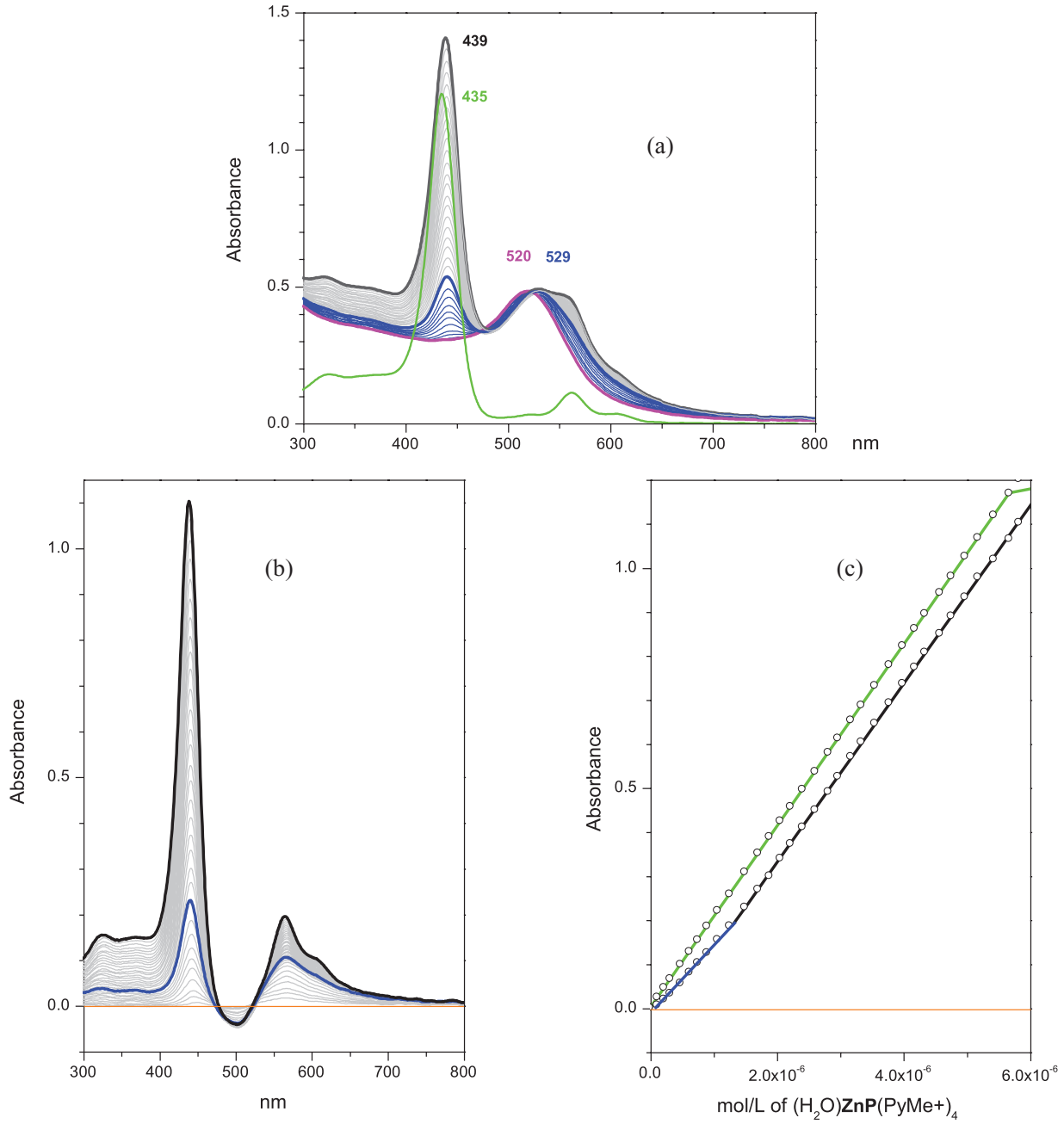

Figure 7 . (a) - Spectral changes in UV-Vis absorption spectra of Au/Cit nanoparticles solution (magenta line) when titration with (H_2O)**ZnP**$(PyMe^+)_4$ tetracations, concentration range is up to $5.86 \cdot 10^{-6}$ mol/l. (b),(c) - corresponding difference spectra obtained by subtracting the initial spectrum of Au/Cit nanoparticles and the nanoparticles absorption at 439 nm in dependence of the tetracation concentration. The formation of the first and second nanoconjugates is highlighted in blue and gray. Free tetracation spectrum with a concentration of $5.86 \cdot 10^{-6}$ mol/L and the absorption changes at 435 nm in dependence of tetracation concentration are shown in green for comparison.

The first compound formation, highlighted in blue, is accompanied by an increase in intensity (ε = 164916) and a red shift of the conjugated tetracation Soret band from 435nm to 439 nm, and the SPR band of the Au/Cit nanoparticle shifts to the red region from 520 to 529 nm. Spectral changes during the sequential formation of two conjugates are checked clearly in the difference absorption spectra obtained by subtracting the initial spectrum of the Au/Cit nanoparticle (Figure 7b). In contrast to the first, the formation of the second conjugate is accompanied only by an increase in the Soret band intensity, while the SPR band has remained about the same, which indicates the lower strength of this product.

The Soret band extinction coefficient of the second conjugate approaches the free tetracation and reaches the value 202115. We did not find any evidence of the reversibility of both conjugates formation, which are formed at a high rate already at the moment of reagents mixing. Both compounds correspond to rectilinear portions on the plots of absorbance dependence at the Soret band maximum from tetracation concentration (Figure 7c), which indicates a constant stoichiometric composition. The stoichiometry of the

first conjugate, calculated at the equivalence point using the Au/Cit nanoparticles extinction coefficient $\varepsilon_{520} = 1.70 \cdot 10^8$,[59,63] is 1 : 454, which appears to have been mistaken. In our opinion, the reason for this error is the overestimated value of the molar extinction coefficient of Au/Cit nanoparticles colloidal solution with a large Au_{30900} nucleus, calculated as for a molecular solution.[73] The geometric sizes ratio of the nanoparticle and the tetracation is shown in Figure 2. Theoretically, the formation of electrostatic conjugates of a colloidal Au/Cit nanoparticle with a sufficiently large number of (H_2O)**ZnP**$(PyMe^+)_4$ tetracations is possible, but we assumed the nanoconjugates with only one tetracation to form first, which reduces nanoparticle ability to further conjugation. The problem of the obtained nanoconjugates stoichiometric composition requires additional studies to determine the extinction coefficients analytical values of AuNC/Cit nanoparticles with an Au_{30900} core, including use of optical porphyrin probes.[74]

Conclusion

Formation of hybrid nanoconjugates of constant composition as a result of interaction between colloidal gold nanoparticles (Au_{30900}) stabilized with citrate and the zinc complex of tetramethylpyridylporphyrin has been established. The molar extinction coefficient of a colloidal solution of large core Au/Cit nanoparticles, calculated for a true molecular solution is unlikely to be a suitable for determining the real stoichiometry of these nanoconjugates. Determining the analytical values of large Au/Cit nanoparticles extinction coefficients requires a new approach. Optical porphyrin probes are seems to be promising analytical reagents for solving this problem.

Acknowledgements. This work was supported by Russian Science Foundation according to the research project № 18-73-00234 (synthesis of zinc complex of *meso*-tetra(N-methyl-4-pyridyl)porphine and experimental investigations of nanoconjugates formation) and by Russian Foundation for Basic Research, research project № 18-53-00035 Bel_a.

References

1. Konan Y.N., Gurny R., Allemann E. *J. Photochem. Photobiol. B* **2002**, *66*, 89–106.
2. Baek S.Y., Na K. *J. Porphyrins Phthalocyanines* **2013**, *17*, 125–134.
3. Vaishnavi E., Renganathan R. *Analyst* **2014**, *139*, 225–234.
4. Wei Y., Zhou F., Zhang D., Chen Q., Xing D. *Nanoscale* **2016**, *8*, 3530–3538.
5. Sheinin V.B., Kulikova O.M., Lipatova I.M., Yusova A.A., Koifman O.I. *Dyes Pigm*. **2018**, *155*, 42–50.
6. Amos-Tautua B.M., Songca S.P., Oluwafemi O.S. *Molecules* **2019**, 24, 2456–2484.
7. Kirar S., Thakur N.S., Laha J.K., Banerjee U.C. *ACS Appl. Bio Mater.* **2019**, *2*, 4202−4212.
8. Khurana R., Kakatkar A.S., Chatterjee S., Barooah N., Kunwar A., Bhasikuttan A.C., Mohanty J. *Front. Chem*. **2019**, *7*, 452.
9. Savacini Sagrillo F., Dias C., Gomes A.T.P.C., Faustino M.A.F., Almeida A., de Souza A.G., Pinto Costa A.R., da Costa Santos Boechat F., de Souza M.C.B.V., Neves M.G.P.M.S., Cavaleiro J.A.S. *Photochem. Photobiol. Sci.* **2019**, *18*, 1910–1922.
10. Singh S., Aggarwal A., Bhupathiraju N.V.S.D.K., Arianna G., Tiwari K., Drain M. C. *Chem. Rev*. **2015**, *115*, 10261−10306.
11. Kataoka H., Nishie H., Hayashi N., Tanaka M., Nomoto A., Yano S., Joh T. *Ann. Transl. Med*. **2017***, 5,* 183.
12. Hong E.J., Choi D.G., Shim M.S. *Acta Pharmaceutica Sinica B*, **2016**, *6*, 297–307.
13. Kou J., Dou D., Yang L. *Oncotarget.* **2017**, *8*, 81591–81603.
14. Chen J.-J., Gao L.-J., Liu T.-J. *Oncol. Lett*. **2016**, *11*, 775–781.
15. Yang N., Tanner J.A., Wang Z., Huang J.-D., Zheng B.-J., Zhua N., Sun H. *Chem. Commun*. **2007**, *42*, 4413–4415.
16. Gorshkova A.S., Rumyantseva V.D., Mironov A.F. *Fine Chemical Technologies* **2018**, *13*, 5–20.
17. Alves E., Costa L., Carvalho C.M.B., Tomé J.P.C., Faustino M.A., Neves M.G.P.M.S., Tomé A.C., Cavaleiro J.A.S., Cunha Â., Almeida A. *BMC Microbiology* **2009**, *9,* 70.
18. Rybachuk G.V. Doctoral Dissertations LSU: Baton Rouge, LA, **2009**, 2545.
19. Vzorov A.N., Dixon D.W., Trommel J.S., Marzilli L.G., Compans R.W. *Antimicrob Agents Chemother* **2002**, *46*, 3917–3925.
20. Vzorov A.N., Marzilli L.G., Compans R.W., Dixon D.W. *Antiviral Res.* **2003,** *59,* 99–109.
21. Kundu S., Patra A. *Chem. Rev*. **2017**, *117,* 712–757.
22. Ibraheam A.S., Al-Douri Y., Voon C.H., Foo K.L., Azizah N., Gopinath S.C.B., Ameri M., Ibrahim S.S. *Appl. Phys. A* **2017**, *123*, 200.
23. Safi M., Domitrovic T., Kapur A., Zhan N., Aldeek F., Johnson J.E., Mattoussi H.. *Bioconjugate Chem*. **2017**, *28,* 64−74.
24. Achadu O.J., Nyokong T. *Spectrochim. Acta, Part A* **2017**, *174*, 339–347.
25. Smykalla L., Mende C., Fronk M., Siles P.F., Hietschold M., Salvan G., Zahn D.R.T., Schmidt O.G., Rüffer T., Lang H. Beilstein J. *Nanotechnol.* **2017**, *8,* 1786–1800.
26. Srivastava S.K., Mittal V. *Hybrid Nanomaterials: Advances in Energy, Environment, and Polymer Nanocomposites*. Scrivener Publishing: Wiley, USA. **2017**, 500 p.
27. *Comprehensive Supramolecular Chemistry II, 2nd Edition* (Atwood J., Ed.), Elsevier: New York **2017**. 4568 p.
28. Ermakova E., Meshkov I., Enakieva Yu., Zvyagina A., Ezhov A., Mikhailov A., Gorbunova Yu., Chernyshev A., Kalinina M., Arslanov V. *Surface Science* **2017**, *660,* 39–46.
29. Huang H.-C., Barua S., Sharma G., Dey S.K., Rege K. *J. Controlled Release* **2011**, *155*, 344–357.
30. Wicki A., Witzigmann D., Balasubramanian V., Huwyler J. *J. Controlled Release* **2015***, 200*, 138–157.
31. Safari J., Zarnegar Z.J. *Saudi Chem. Soc*. **2014**, *18,* 85–99.
32. Li W., Cao Z., Liu R., Liu L., Li H., Li X., Chen Y., Lu C., Liu Y. *Artificial Cells, Nanomedicine, and Biotechnology* **2019**, *47*, 4222–4233.
33. Du J.Z., Li H.J., Wang J. *Acc Chem Res.* **2018**, *51*, 2848–2856.
34. Melamed J.R., Riley R.S., Valcourt D.M., *et al. ACS Nano* **2016**, *10*, 10631–10635.
35. Sood R., Chopra D.S. *Materials Sci. Eng. C, Mater.* **2018**, *92*, 575–589.
36. Tang Y., Liang J., Wu A., *et al. ACS Appl. Mater. Interfaces*. **2017**, *9,* 26648–26664.
37. Al-Dhabi N.A., Ghilan A.M., Arasu M.V., *et al. J. Photochem. Photobiol. B, Biol*. **2018**, *189,* 176–184.
38. Pompa P.P., Martiradonna L. *et al. Nature Nanotechnology* **2006**, *1,* 126–130.
39. Gamaleia N.F., Shton I.O. *Photodiagnosis and Photodynamic Therapy* **2015***, 12*, 221–231.
40. Shibu E.S., Hamada M., Murase N., *et al. J. Photochem. Photobiol, C: Photochem. Rev.* **2013**, *15*, 53–72.

41. Kim S.B., Lee T.H., Yoon I. *et al. Chem. Asian J.* **2015***, 10*, 563–567.
42. Moeno S., Antunes E., Nyokong T. *J. Photochem. Photobiol. A: Chem.* **2011**, *222,* 343–50.
43. Wieder M.E., Hone D.C., Cook M.J., *et al. Photochem. Photobiol. Sci.* **2006**, *5*, 727–734.
44. Camerin M., Magaraggia M., Soncin M., *et al. Eur. J. Cancer* **2010**, *46*, 1910–1918.
45. Stuchinskaya T., Moreno M., Cook M.J., *et al. Photochem. Photobiol. Sci.* **2011**, *10*, 822–831.
46. Cheng Y., Samia A.C., Meyers J.D., *et al. J. Am. Chem. Soc.* **2008**, *130*, 10643–10647.
47. Cheng Y., Meyers J.D., Agnes R.S., *et al. Small* **2011**, *7*, 2301–2306.
48. Cheng Y., Doane T.L., Chuang C.H., *et al. Small* **2014**, *10*, 1799–1804.
49. Terentyuk G., Panfilova E., Khanadeev V., *et al. Nano Res*. **2014**, *7*, 325–337.
50. Zhao T., Yu K., Li L., *et al. ACS Appl. Mater. Interfaces* **2014**, *6*, 2700–2708.
51. Gamaleia N.F., Shishko E.D., Shton I.O., *et al. Photobiol. Photomed.* **2012,** *9*, 94–98.
52. Gamaleia N.F., Dolinsky G.A, Shishko E.D, *et al. Forum Immunopathol. Dis. Therap.* **2011***, 2*, 237–246.
53. Zhou Y., Liang X., Dai Z. *Nanoscale* **2016**, *8*, 12394–12405.
54. Hambright P., Gore T., Burton M. *Inorg. Chem.* **I976**, *15*, 2314–2315.
55. Sugata S., Yamanouchi S., Matsushima Y. *Chem. Pharm. Bull.* **1977**, *25*, 884–889.
56. Bailey S.L., Hambright P. *Inorg. Chim. Acta* **2003**, *344,* 43–48.
57. Ishikawa Y., Yamakawa N., Uno T. *Bioorg. Med. Chem*. **2007**, *15*, 5230–5238.
58. Frens G. *Nature*: *Phys. Sci.* **1973**, *241*, 20–22.
59. Panteleev A.V., Vavulin D.N., Alfimov A.V., Andreeva O.V., Aryslanova E.M., Chivilikhin S.A. *Nanosystems: Physics, Chemistry, Mathematics* [*Наносистемы: Физика, Химия, Математика]* **2012**, *3*, 123–133 (in Russ.).
60. Sheinin V.B., Kulikova O.M., Koifman O.I. *J. Mol. Liq.* **2019**, *277*, 397–408.
61. Haiss W., Thanh N.T.K., Aveyard J. *Anal. Chem*. **2007**, *79*, 14215–4221.
62. Rahman S. *Undergraduate Journal of Mathematical Modeling: One + Two* **2016**, *7*(1), art. 2.
63. Holec D., Dumitraschkewitz P., Vollath D., Fischer F.D. *Nanomaterials* **2020**, *10,* 484.
64. Goldberg R.N., Kishore N., Lennen R.M. *J. Phys. Chem. Ref. Data* **2002**, *31,* 231–370.
65. Silva A.M.N., Kong X., Hider R.C. *Biometals* **2009**, *22*, 771–778.
66. Park J.-W., Shumaker-Parry J.S. *J. Am. Chem. Soc*. **2014**, *136*, 1907−1921.
67. Al-Johani H., Abou-Hamad E., Jedidi A., Widdifield C.M., Viger-Gravel J., Sangaru S.S. Basset J.-M. *Nature Chemistry* **2017**, *9,* 890–895.
68. Park J.-W. *Part. Syst. Charact*. **2019**, *36,* 1800329. 1–9.
69. Contreras-Trigo B., Díaz-García V., Guzmán-Gutierrez E., Sanhueza I., Coelho P., Godoy S., Torres S., Oyarzún P. *Sensors* **2018**, *18*, 2246.
70. Toma H.E., Zamarion V.M., Toma S.H., Araki K. *J. Brazilian Chem. Soc.* **2010**, *21*, 1158–1176.
71. Mikros E., Gaudemer A., Pasternack R. *Inorg. Chim. Acta* **1988**, *153,* 199–200.
72. Hambright P., Fleisher E. B. *Inorg. Chem*. **1970**, *9*, 1757–1761.
73. Shang J., Gao X. *Chem. Soc. Rev*. **2014,** *43*, 7267–7278.
74. Sheinin V.B., Kulikova O., Zenkevich E.I., Selyshchev O., Dzhagan V., Stroyuk A., Raevskaya A., Koifman O.I., Zahn D.R.T. *Abstracts of 1st Int. Conferences on Noncovalent Interactions (ICNI-2019)*, September 1–6, **2019**, Lisbon, Portugal, P. 82.

Received 15.05.2020
Accepted 15.01.2021